bioRxiv preprint doi: https://doi.org/10.1101/2021.10.25.465733; this version posted June 9, 2022. The copyright holder for this preprint (which was not certified by peer review) is the author/funder, who has granted bioRxiv a license to display the preprint in perpetuity. It is made available under aCC-BY-ND 4.0 International license.

IntAct: a non-disruptive internal tagging strategy to study actin isoform organization and function

M.C. van Zwam[1], W. Bosman[1,*], W. van Straaten[1,*], S. Weijers[1], E. Seta[1], B. Joosten[1], and K. van den Dries[1,✉]

[1]Department of Cell Biology, Radboud Institute for Molecular Life Sciences, Radboud University Medical Center, Nijmegen, The Netherlands
[*]Contributed equally

Actin plays a central role in many cell biological processes including division and motility. Mammals have six, highly conserved actin isoforms with nonredundant biological functions, yet the molecular basis of isoform specificity remains elusive due to a lack of tools. Here, we describe the development of IntAct, an internal tagging strategy to study actin isoform function in fixed and living cells. We first identified a residue pair in β-actin that permits non-disruptive tag integration. Next, we used knock-in cell lines to demonstrate that the expression and filament incorporation of IntAct β-actin is indistinguishable from wildtype. Also, IntAct β-actin remains associated with the actin-binding proteins profilin and cofilin and can be targeted in living cells. To demonstrate isoform-specificity, we generated IntAct γ-actin cells and demonstrate that characteristic actin isoform localization remains unaltered. Together, our data demonstrate that IntAct is a versatile tool to study actin isoform localization, dynamics and molecular interactions.

Actin isoforms | Cytoskeleton | Protein engineering | Microscopy
Correspondence: ***Koen.vandenDries@radboudumc.nl***

Introduction

Actin plays a central role during fundamental biological processes including cell division, shape maintenance, motility and contractility. In birds and mammals, actin has six isoforms, also called isoactins, which are encoded by different genes and expressed in a tissue and time-specific manner during development, homeostasis and pathology (1–3). All six isoactins have nonredundant functions as indicated by the discovery of disease-causing mutations in each of the genes encoding the isoforms (4). Although exceptions exist, it is generally acknowledged that four isoactins are expressed in muscle cells and two are ubiquitously expressed across tissues. The two ubiquitous isoactins, nonmuscle β- and γ-actin, display the highest similarity with only four different residues at their N-terminus (5). Despite this similarity, nonmuscle β- and γ-actin play specific roles in many actin-controlled processes including cell-cell junction formation (6), axon development (7), cell division (8, 9) and cell migration (10, 11). While it has been demonstrated that isoactin-specific posttranslational modification (12, 13), nucleation (8, 9) and translation speed (13, 14) contribute to the nonredundant role of β- and γ-actin in cellular processes, the molecular principles that govern the differential function of isoactins remain largely unclear. This is primarily due to the limited possibilities to specifically probe actin isoforms for biochemical and cell biological assays.

Common tools to label the actin cytoskeleton such as phalloidin (15) in fixed cells or Lifeact (16), F-tractin (17), UtrophinCH (18), and anti-actin nanobodies (19–21) in living cells do not discriminate between isoactins. Furthermore, C-terminal fusions of actin cannot be used to study isoactin biology since they only poorly assemble into filaments (22, 23). N-terminal fusions of actin have been used to study isoactin differences in cells (14, 24, 25), but the reporter tags are known to significantly interfere with actin dynamics (16), nucleation (26) and molecular interactions (16, 26–28). Moreover, N-terminal fusion prevents isoactin-specific and nonspecific posttranslational modifications crucial for proper actin function such as arginylation (12, 13) and acetylation (29, 30). Attempts to tag yeast actin internally with a tetracysteine tag for contractile ring visualization were unsuccessful since none of the modified actins were integrated into the contractile ring filaments (31). An extended search for other internal sites that may be permissive for epitope tagging of actin has not been performed so far.

Here, we describe the development of a non-disruptive internal tagging strategy to study isoactin organization and function, which we call IntAct. For this, we first performed a microscopy-based screen for eleven internal actin positions and identified one residue pair that allows non-disruptive epitope tagging of actin. To prove its versatility and usability, we engineered CRISPR/Cas9-mediated knock-in cell lines with various antibody- and nanobody-based epitope tags in the identified position and demonstrate that the internally tagged actins are properly expressed and that the integration into filaments is unperturbed. By performing immunofluorescence, pulldown experiments and live-cell imaging with the internally tagged actins, we show that IntAct can be used to study actin localization, molecular interactions and dynamics. Lastly, we show that isoactin-specific localization of nonmuscle β- and γ-actin appears unaffected, strongly suggesting that IntAct can provide unique insight into the isoactin-specific molecular principles that regulate cellular processes such as division, motility, and contractility.

Results

T229/A230 actin residue pair is permissive for epitope tag insertion. To identify a permissive residue pair to internally tag the actin protein, we first performed a medium-scale

bioRxiv preprint doi: https://doi.org/10.1101/2021.10.25.465733; this version posted June 9, 2022. The copyright holder for this preprint (which was not certified by peer review) is the author/funder, who has granted bioRxiv a license to display the preprint in perpetuity. It is made available under aCC-BY-ND 4.0 International license.

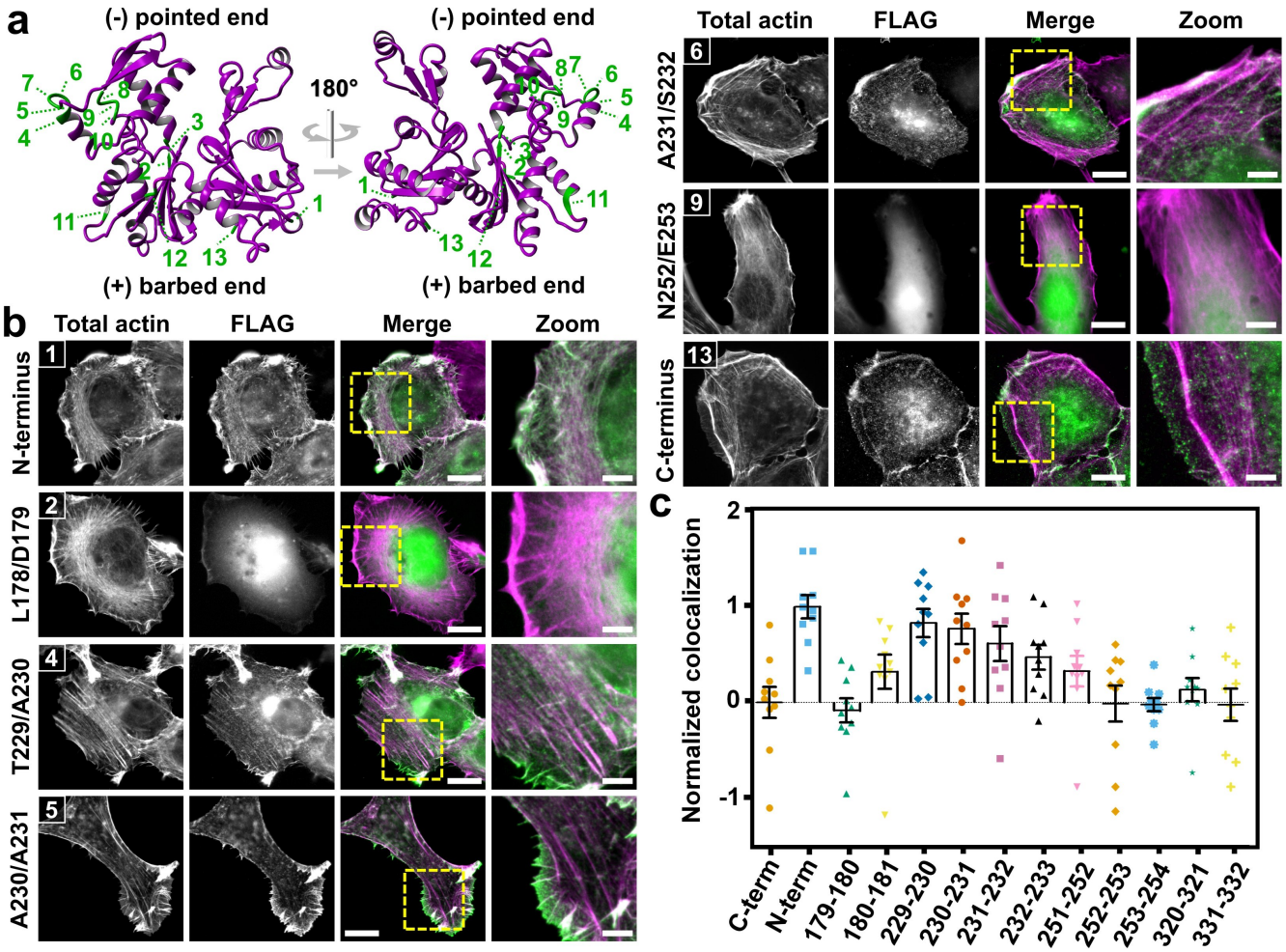

Fig. 1. Identification of actin T229/A230 as a permissive target site for epitope tag integration a, Crystal structure of uncomplexed globular actin (magenta ribbon, PBD accession number: 1J6Z (32)) indicating the eleven internal target positions (green) as well as the N- and the C-terminus (1 and 13, respectively). **b,** Representative widefield immunofluorescence images of total actin (magenta) and FLAG (green) in HT1080 cells that overexpress the tagged β-actin variants. Shown are five internally tagged variants and the N- and C-terminally tagged β-actin. The remaining six internally tagged variants are shown in **Suppl. Fig. S1**. Scale bar: 15 µm. Scale bar zoom: 5 µm. **c,** Colocalization analysis of the microscopy results in b showing the normalized Pearson's coefficient for each of the actin variants. Individual data points indicate single cells and in total, at least 10 cells from 2 independent experiments were included in the analysis. Bars represent the mean value, and error bars represent standard error of mean (SEM).

screen and tagged β-actin at eleven distinct residue pairs with a FLAG tag (**Fig. 1a**). These residue pairs were carefully selected, ensuring that at least one of the residues is part of an unstructured region (32) and that both residues were not involved in F-actin interactions (33). Furthermore, the first 40 residues were avoided since the coding mRNA for this region is involved in the different translation kinetics of actin isoforms (13). Eventually, two of the eleven selected positions were located in subdomain 3, seven in subdomain 4, and two were close to the ATP binding site. C- and N-terminally tagged β-actin were included in the screen as a negative and positive control for filament integration, respectively. We chose the FLAG tag as an epitope for our screen because of its frequent use, small size (8 amino acids, DYKDDDDK), and availability of a highly specific and well-characterized antibody (34).

To evaluate the integration of the tagged actins within the actin cytoskeleton, we overexpressed the thirteen actin variants in human fibrosarcoma cells (HT1080, **Fig. 1b-c, Fig. S1**) and retinal pigment epithelium cells (RPE1, **Fig. S2**) and performed an immunofluorescence staining for the FLAG tag and phalloidin as a total F-actin marker (**Fig. 1b, Fig. S1, Fig. S2**). Interestingly, by visual inspection, we observed that most of the internally tagged actins were diffusely present within the cytosol with two notable exceptions (T229/A230 and A230/A231). Of these two variants, A230/A231 only seemed to present a clear overlap with total actin at the cell periphery but the T229/A230 overlapped almost entirely with the total actin signal, similar to N-terminally tagged actin. To quantitatively assess the colocalization of the tagged actin variants with F-actin, we performed a Pearson correlation coefficient analysis (**Fig. 1c, Fig. S2b**). As expected, N-terminally tagged actin showed a high degree of colocalization, while C-terminally tagged actin showed almost no colocalization. We therefore performed a unity-based normalization, adjusting the Pearson coefficient of the C- and N-terminus to zero and one, respectively, and normalized the other values within this window.

bioRxiv preprint doi: https://doi.org/10.1101/2021.10.25.465733; this version posted June 9, 2022. The copyright holder for this preprint (which was not certified by peer review) is the author/funder, who has granted bioRxiv a license to display the preprint in perpetuity. It is made available under aCC-BY-ND 4.0 International license.

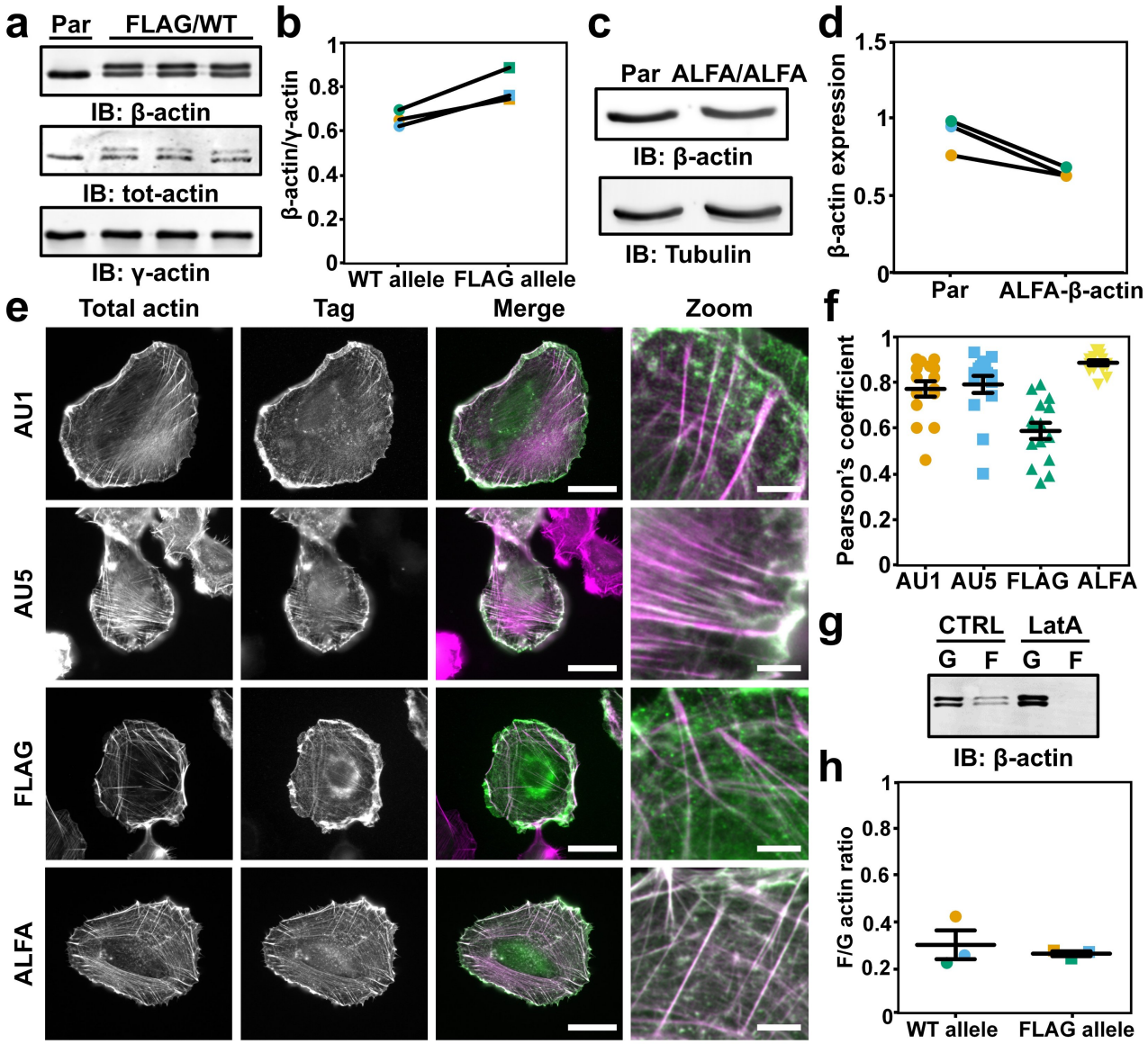

Fig. 2. Actin functionality unperturbed by T229/A230 epitope integration a, Western blot of β-actin, total actin and γ-actin in parental HT1080 (Par) and 3 independent heterozygous FLAG-β-actin HT1080 clones (FLAG/WT). **b,** Quantification of β-actin protein expressed by the WT allele and the FLAG allele as shown in a and normalized to γ-actin. **c,** Representative western blot showing β-actin expression in parental HT1080 (Par) and homozygous ALFA-β-actin HT1080 cells (ALFA/ALFA). **d,** Quantification of the β-actin expression from the western blot shown in **c** and normalized to tubulin. **e,** Representative widefield images from cells that have a CRISPR/Cas9-mediated knock-in of AU1, AU5, FLAG or ALFA tag in β-actin. Cells were labeled for phalloidin and an antibody/nanobody against the respective tag to visualize total actin (magenta) and the tagged β-actin (green). Scale bar: 15 µm. Scale bar zoom: 5 µm. **f,** Colocalization analysis of the microscopy results in **e** showing the Pearson's coefficient for each of the internally tagged actins. Individual data points indicate single cells and in total, at least 10 cells from 2 independent experiments were included in the analysis. Bars represent the mean value, and error bars represent standard error of mean (SEM). **g,** Representative western blot of G-actin and F-actin fraction in heterozygous FLAG-β-actin HT1080 cells that were left untreated or treated with latrunculin A. **h,** Quantification of the F-/G-actin ratio for β-actin expressed by the WT allele and FLAG allele from the western blots shown in g. Bars represent the mean value, and error bars represent standard error of mean (SEM).

While most of the internally tagged actin variants showed little to no colocalization, the T229/A230 variant displayed a high Pearson coefficient in both HT1080 and RPE1 cells (raw R^2=0.68 and 0.75, respectively). The colocalization analysis therefore confirms our initial observation and strongly suggest that the T229/A230 residue pair in β-actin is permissive for epitope tag insertion without affecting the ability of actin to be incorporated within filaments.

T229/A230 epitope tag insertion does not impair actin expression or assembly into filaments. To investigate the versatility and usability of the T229/A230 residue pair for epitope tag insertion, we applied CRISPR/Cas9-mediated homology-directed repair (HDR) to genetically introduce various tags into this position at the genomic locus of β-actin. We included the antibody-based epitope tags FLAG (DYKDDDDK), AU1 (DTYRYI) and AU5 (TDFYLK) as well as the recently developed nanobody(Nb)-based ALFA tag (PSRLEEELRRRLTEP) (35). Of note, we introduced the AU5 tag without the starting threonine (DFYLK), since this residue is redundant with the T229 of actin. Eventually, we obtained cells with at least one properly modified allele for AU1, AU5 and FLAG, and homozygous knock-in cells for the ALFA tag as confirmed by Sanger sequencing (**Fig. S3**).

bioRxiv preprint doi: https://doi.org/10.1101/2021.10.25.465733; this version posted June 9, 2022. The copyright holder for this preprint (which was not certified by peer review) is the author/funder, who has granted bioRxiv a license to display the preprint in perpetuity. It is made available under aCC-BY-ND 4.0 International license.

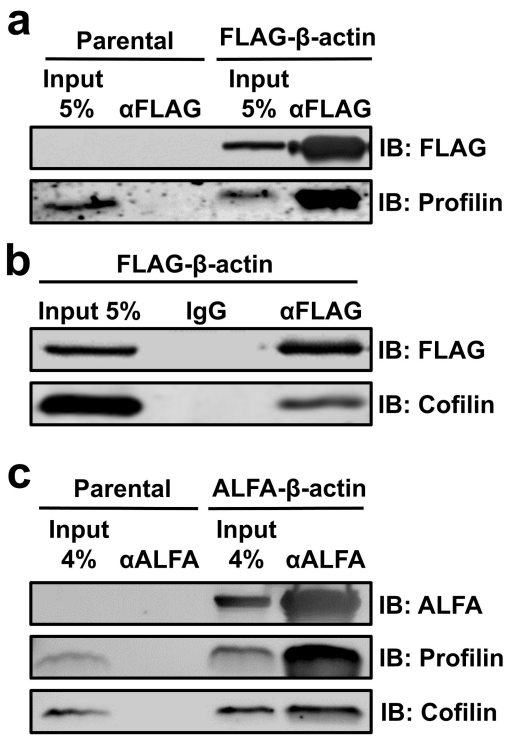

Fig. 3. FLAG- and ALFA-β-actin interact with profilin and cofilin a, Representative western blot showing the co-immunoprecipitation of FLAG-β-actin and profilin using an anti-FLAG antibody in the FLAG-β-actin HT1080 cells. Co-immunoprecipitation performed on parental HT1080 was included as a control. **b,** Representative western blot showing the co-immunoprecipitation of FLAG-β-actin and cofilin using an anti-FLAG antibody. IgG was included as a negative control. **c,** Representative western blot showing the co-immunoprecipitation of ALFA-β-actin and profilin and cofilin using an anti-ALFA nanobody in the ALFA-β-actin HT1080 cells. Co-immunoprecipitation performed on parental HT1080 was included as a control.

After generation of the knock-in cells, we first evaluated actin protein expression. For this, we used heterozygous FLAG-β-actin cells since FLAG causes a gel shift on western blot, allowing a direct comparison of tagged and wildtype actin expression in the same cells. Quantification of the western blots demonstrated that the amount of FLAG-β-actin was similar to wildtype indicating that the cells did not downregulate the expression of β-actin from the knock-in allele (**Fig. 2a-b**). We also evaluated actin protein expression in the homozygous ALFA-β-actin cells and this showed that the total amount of actin was slightly lower in the ALFA-β-actin cells compared to parental HT1080 cells (**Fig. 2c-d**). Although we expect that this decrease is attributed to clonal variation, we wanted to exclude compromised global actin regulation in the ALFA-β-actin cells. We therefore evaluated the expression of γ-actin and α-smooth muscle actin (α-SMA) since a genetic loss of β-actin has been shown to induce the expression of these isoforms (36). Importantly, we neither observed differences in γ-actin expression or an induction of α-SMA in the ALFA-β-actin cells (**Fig. S4**), strongly suggesting that global actin regulation is not perturbed by genetically tagging β-actin.

Next, we assessed the incorporation of the tagged actins into the cytoskeleton by performing immunofluorescence labeling followed by widefield microscopy (**Fig. 2e**). Pearson colocalization analysis demonstrated that all the knock-in tagged actins have a strong overlap with F-actin, indicating that they are well incorporated in actin filaments (**Fig. 2f**). Since the ALFA tag allows intracellular detection of the tagged actins in living cells, we also performed live-cell imaging with the ALFA-β-actin cells. For this, we overexpressed ALFA-Nb-mScarlet in the ALFA-β-actin cells and evaluated its colocalization with F-actin by co-transfecting Lifeact-GFP and determining the Pearson's coefficient at multiple time points (**Fig. S5, Suppl. Movie 1**). This demonstrated that, also in living cells, there is a very high correlation (R^2=>0.8) between the fluorescence intensity of the tagged actins and the Lifeact-GFP signal (**Fig. S5b**). This further supports the notion that the T229/A230 internally tagged β-actin is properly assembled into actin filaments.

To corroborate our microscopy results, we sought to biochemically determine the F/G-actin ratio of the tagged and wildtype actin and for this, we again used the heterozygous FLAG-β-actin cells. F-actin was obtained using high speed centrifugation and cells stimulated with Latrunculin A to disrupt F-actin were included as a negative control (**Fig. 2g**). The results from these experiments demonstrated that the F/G-actin ratio for FLAG-β-actin was indistinguishable from wildtype actin (**Fig. 2h**), indicating that FLAG-β-actin was normally integrated into actin filaments.

Together, these results in fixed and living cells with multiple epitope tags suggest that the T229/A230 residue pair in actin is a versatile position for epitope tagging with only a minor impact on actin expression and no measurable effect on the ability of actin to integrate into filaments.

Internally tagged actins interact with cofilin and profilin. To study the molecular interactions of the internally tagged β-actin, we performed a co-immunoprecipitation assay and western blot analysis using FLAG-β-actin and ALFA-β-actin. Since co-immunoprecipitation of actin only allows the investigation of monomeric G-actin interactors, we evaluated the binding of the well-established G-actin binding proteins cofilin and profilin. From the results, we first concluded that both FLAG- and ALFA-β-actin could be immunoprecipitated from the lysates (**Fig. 3a-c**), thereby confirming the availability of the epitope tags under native conditions. More importantly, we could also demonstrate that FLAG-β-actin (**Fig. 3a-b**) as well as ALFA-β-actin (**Fig. 3c**) still associate with cofilin and profilin, indicating that the internally tagged actins maintain their ability to bind to these important actin regulators.

Actin retrograde flow and cell function is unperturbed in ALFA-β-actin cells. Fluorescent fusions of actin are known to affect actin retrograde flow at the cell front, likely due to the large fluorescent reporter tag (16). To evaluate whether actin retrograde flow is unperturbed by introducing the internal tag at position T229/A230, we determined the actin flow at lamellipodia using live cell imaging (**Fig 4a**). For this, we transfected ALFA-β-actin cells with Lifeact-GFP or ALFA-Nb-GFP and performed time lapse imaging with Airyscan super-resolution microscopy. Parental cells trans-

bioRxiv preprint doi: https://doi.org/10.1101/2021.10.25.465733; this version posted June 9, 2022. The copyright holder for this preprint (which was not certified by peer review) is the author/funder, who has granted bioRxiv a license to display the preprint in perpetuity. It is made available under aCC-BY-ND 4.0 International license.

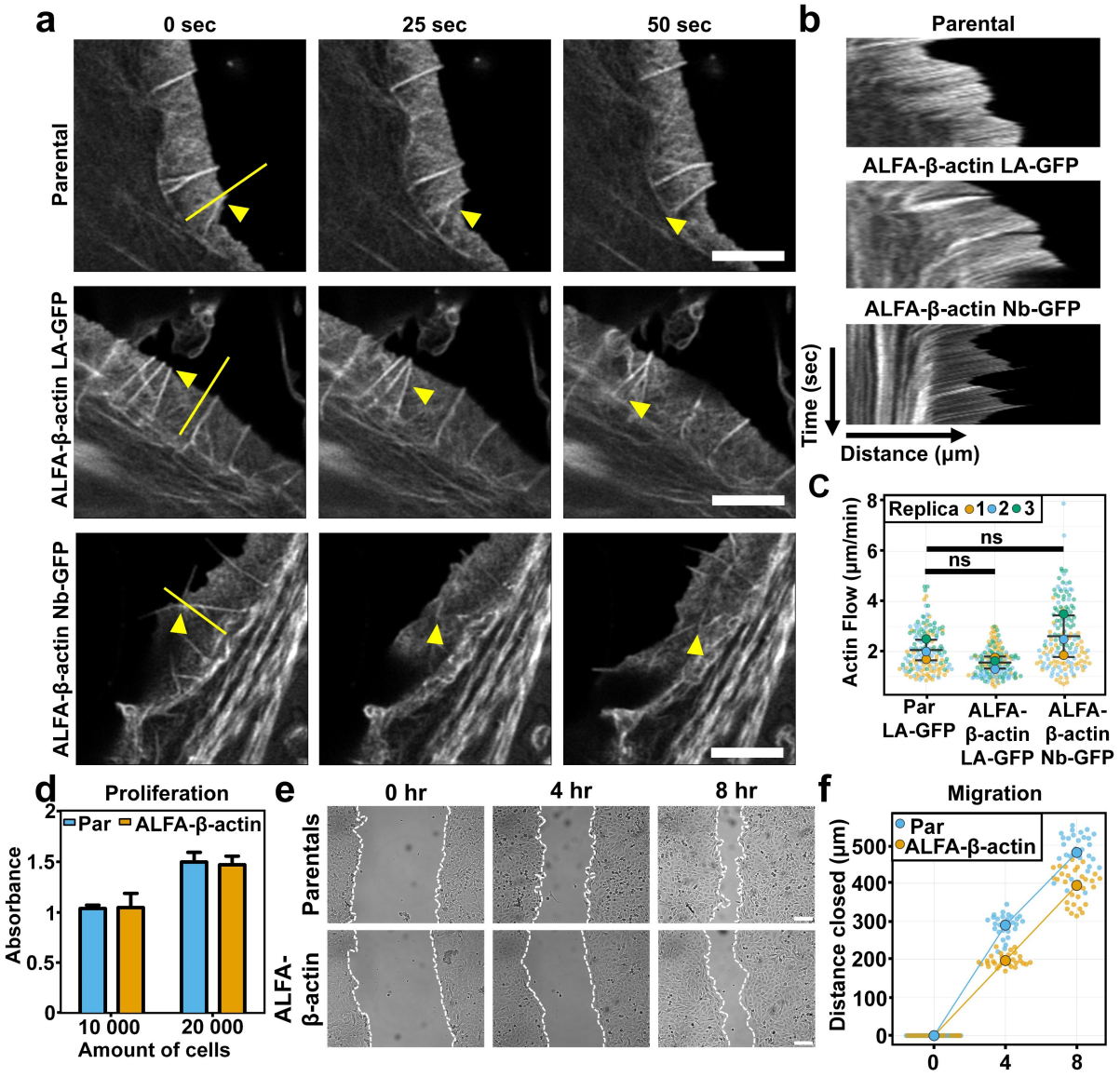

Fig. 4. Actin retrograde flow and cell proliferation and migration are not affected by β-actin internal tagging a, Representative airyscan images of HT1080 parental cells transfected with Lifeact-GFP (LA-GFP), HT1080 ALFA-β-actin cells transfected with Lifeact-GFP and HT1080 ALFA-β-actin cells transfected with ALFA-Nb-GFP. Shown are three stills and the yellow triangles indicate actin features that display retrograde flow. Yellow line indicates the position of kymographs shown in **b**. The full movies are available as **Suppl. Movies 2-4**. Scale bar: 4 µm. **b,** Representative kymographs of parental, ALFA-β-actin-LA-GFP and ALFA-β-actin-Nb-GFP as indicated by the yellow line in **a**. **c,** Quantification of the actin retrograde flow (µm/min) in parentals-LA-GFP, ALFA-β-actin-LA-GFP, ALFA-β actin-Nb-GFP. Large datapoints represent the average for each experiment and the small datapoints represent individual kymographs. The bars show the median and the error bars represents standard deviation. Statistical analysis was performed using unpaired Welch's t-test. Parentals-LA-GFP vs ALFA-β-actin-LA-GFP P=0.16. Parentals-LA-GFP vs ALFA-β-actin-Nb-GFP P=0.38. **d,** Quantification of a MTT proliferation assay performed on parental and ALFA-β-actin HT1080 cells. Bars represent the mean value, and error bars represent standard error of mean (SEM) of 3 experiments. **e,** Representative widefield images of parental and ALFA-β-actin HT1080 cells at time point 0 hr, 4 hr and 8 hr after scratch induction. Scale bar: 30 µm. **f,** Quantification of the scratch assay shown in **e** indicating the distance closed in µm over time in parental (Par) and ALFA-β-actin HT1080 cells. Large data points represent the mean of 2 experiments and the small data points represent the quantification of the individual images. 15 images per condition were acquired per experiment.

fected with Lifeact-GFP were included as a control since the expression of Lifeact has been demonstrated to not affect the actin retrograde flow at the cell front (16). Importantly, we observed actin flow at lamellipodia in all of the conditions indicating no gross defects in the formation of these structures by the internal ALFA tag (**Suppl. Movie S2-4**). Moreover, by quantitative analysis of the kymographs from the time-lapse videos, we demonstrate that there are no significant differences in actin flow at lamellipodia between any of the investigated conditions (**Fig. 4b-c**). These results strongly suggest that actin dynamics is not disturbed by the internal tag in β-actin or the overexpression of the ALFA-Nb-GFP.

To demonstrate that the internal tag does not influence cellular processes that are crucially dependent on proper actin function, we evaluated the ability of ALFA-β-actin cells to proliferate and migrate as compared to parental HT1080 cells. To assess cell proliferation, we performed a MTT assay and observed no differences in the the proliferation rate between ALFA-β-actin and parental HT1080 cells (**Fig. 4d**). To assess cell migration, we performed a scratch assay. Althoug the migration rate of the ALFA-β-actin cells was slightly lower compared to parental HT1080 cells, these cells still

bioRxiv preprint doi: https://doi.org/10.1101/2021.10.25.465733; this version posted June 9, 2022. The copyright holder for this preprint (which was not certified by peer review) is the author/funder, who has granted bioRxiv a license to display the preprint in perpetuity. It is made available under aCC-BY-ND 4.0 International license.

closed the scratch wound and the minor difference in migration speed was only observed in the first 4 hrs (**Fig. 4e-f**).

Together, these results indicate that actin dynamics as well as major actin-dependent cellular functions are largely unaffected when actin is tagged at postion T229/A230.

Tagged β- and γ-actin recapitulate differential isoform distribution. So far, our results strongly suggest that the T229/A230 position in actin is a permissive position for non-disruptive epitope tag integration. We term this internal tagging strategy "IntAct" and propose that it can be used to study the molecular principles of actin isoform specificity in biological processes. To indeed demonstrate that the tagged actins recapitulate the behaviour of wildtype isoforms, we also engineered HT1080 IntAct knock-in cells with an ALFA tag in the genomic locus of the ubiquitously expressed isoform γ-actin. Since it has been shown before that β- and γ-actin display a differential cellular distribution (11, 37), we evaluated whether the localization of these isoforms is similar in parental and IntAct HT1080 cells. For this, we labelled parental cells with isoform-specific antibodies, and the IntAct cells with an anti-ALFA nanobody as well as phalloidin for normalization. Cells were imaged with Airyscan microscopy and the distribution of actin isoforms was evaluated through ratio calculations. In line with previous observations, we first found that in the parental HT1080 cells, β-actin is enriched at the cell cortex and γ-actin is enriched in stress fibers (**Fig. 5a-d**). More importantly, we clearly noted that also in the IntAct HT1080 cells, β- and γ-actin displayed a differential distribution with β-actin being more strongly present at the cortex and γ-actin at the stress fibers (**Fig. 5e-f**). Together, these results indicate that isoform-specific properties remain preserved after internal tagging at position T229/A230.

Discussion

In this manuscript, we present a strategy to internally tag actin without disrupting its function. At this point, we can only speculate as to why the T229/A230 position seems permissive for manipulation. The T229/A230 residue pair is located in subdomain 4 and is part of a region that has been termed the V-stretch due to the high structural variation that this region exhibits in molecular dynamics simulations of F-actin (38). To the best of our knowledge, the V-stretch has no explicitly described interactions with actin-binding proteins and, unlike other variable regions such as the D-loop, is not involved in interactions between monomers in actin filaments (39). An alanine mutagenesis scan of the entire β-actin protein further demonstrated that the V-stretch has a high structural plasticity since the alanine mutants covering this region were not impaired in their folding capacity or their binding to the actin-binding proteins DNAse I, adseverin, Thymosin β4 and CAP (40). It must be noted though that the T229/A230 residue pair is very close to the proposed binding interface of the actin-binding protein nebulin, and therefore possibly also the related protein nebulette (41). Nonetheless, since nebulin and nebulette are exclusively present in skeletal and cardiac muscle, respectively, we expect this will not be an obstacle for studying the non-muscle and smooth muscle actin isoforms. Future investigations using internally tagged α-skeletal or α-cardiac actin, however, need to carefully control for the possibility that the binding with nebulin or nebulette is influenced by the use of the T229/A230 residue pair.

A previous attempt to internally tag actin with a tetracysteine tag in yeast demonstrated that, out of eight different internal sites, only the S232/S233 position allowed weak assembly of actin into filament cables (31). The fact that the internal position identified by us is extremely close to this S232/S233 residue pair further indicates that this region is relatively permissive for manipulation. Interestingly, in our screen, we also included the S232/S233 residue pair as well as the other two adjacent positions, i.e. A230/A231 and A231/S232. These internally tagged variants, however, were not as well assembled into filaments as the T229/A230 variant, suggesting very specific structural requirements for actin internal tagging.

In summary, our results demonstrate that the T229/A230 residue pair allows internal tagging of actin, which can be used to study the localization and dynamics of specific actin isoforms. Also, we show that this internal tagging strategy enables the investigation of molecular interactions of monomeric actin using standard pulldown assays. Interestingly, since our approach involves intracellular targeting of specific actin variants, we envision that fusing the anti-ALFA nanobody with peroxidases (e.g. APEX2 (42)) or biotin ligases (e.g. TurboID (43)) will allow the future investigation of isoactin-specific molecular interactions of both monomeric and filamentous actin. Based on the high conservation of actin from yeast to mammals, we further expect that this internal position can be used to study differences of actin variants across species. Finally, by tagging mutant actin variants, our approach could also open avenues to unravel the disease causing mechanisms of a wide variety of actinopathies (4), for which currently no strategy is available.

Experimental Procedures

Cell Culture. HT1080 fibrosarcoma cells were used for the overexpression of internally tagged actins and to generate the internally tagged cell lines. Cells were cultured in 1x DMEM + 4.5 g/L D-Glucose, NEAA (Gibco, Lot#2246377) and supplemented with 10% (vol/vol) fetal bovine serum (FBS), 1X Glutamax (Gibco, 2063631), 1 mM Sodium Pyruvate (Gibco, 2010382) and 0.5X Antibiotic-Antimycotic (Gibco, 15240-062). RPE1 cells were used for the overexpression of internally tagged actins. RPE1 cells were cultered in advanced DMEM/F-12 + non-essential amino acids + 110mg/L Sodium Puruvate (Gibco, Lot#12634010) supplemented with 10% (vol/vol) fetal bovine serum (FBS) and 1X Glutamax (Gibco, 2063631). All cell lines were cultured and kept at 37°C with 5% CO2.

Antibodies and reagents. The following primary antibodies were used: anti-β-actin (#MCA5775GA, Bio-Rad Laboratories, 1:100 for immunofluorescence, 1:1000 for

bioRxiv preprint doi: https://doi.org/10.1101/2021.10.25.465733; this version posted June 9, 2022. The copyright holder for this preprint (which was not certified by peer review) is the author/funder, who has granted bioRxiv a license to display the preprint in perpetuity. It is made available under aCC-BY-ND 4.0 International license.

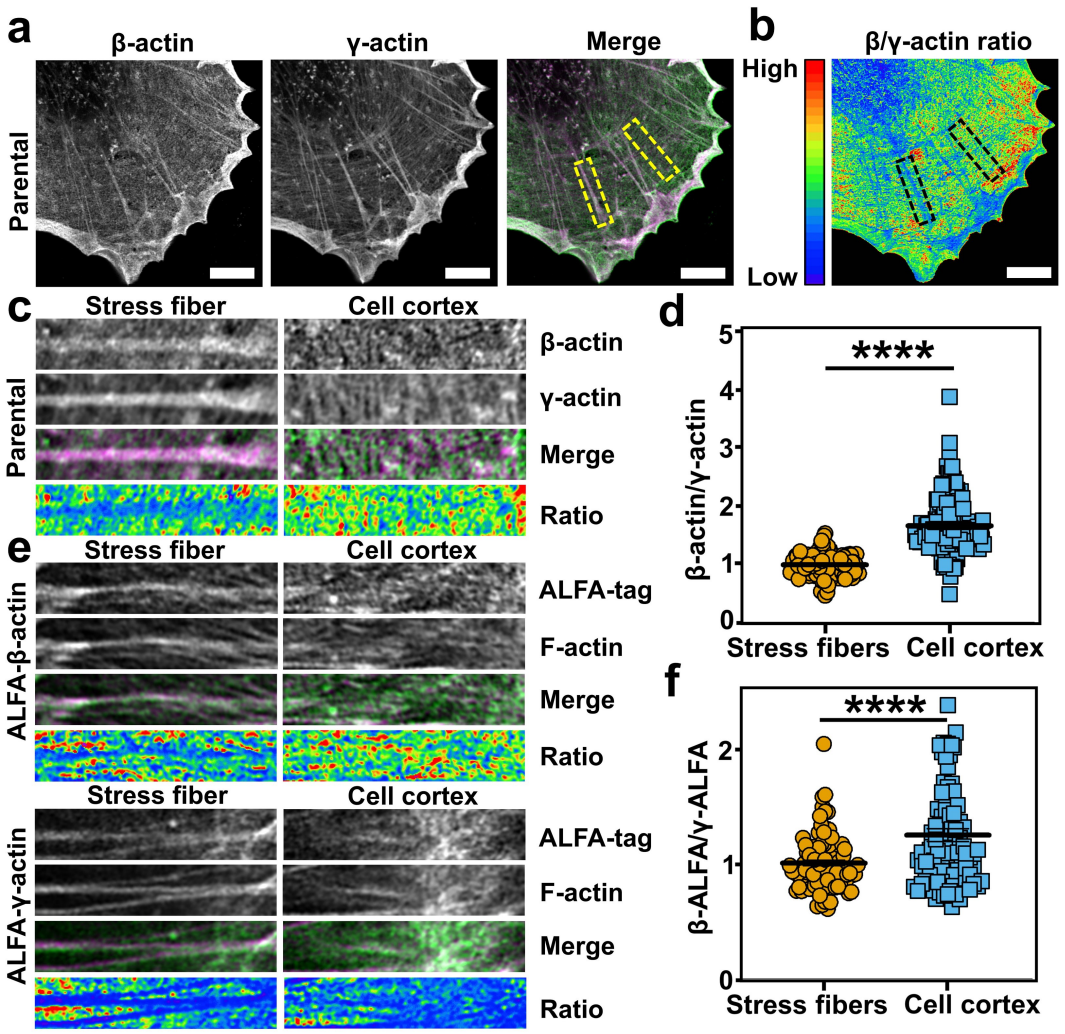

Fig. 5. IntAct β- and γ-actin recapitulate differential distribution of actin isoforms a, Representative Airyscan images of parental HT1080 stained for β-actin (green) and γ-actin (magenta). Scale bar: 5 µm. **b,** 32-Color ratio image of β-actin divided by γ-actin for the cell shown in **a**. Scale bar: 5 µm. **c,** Representative images of selected regions of interest of stress fibers (left column) and cell cortex (right column) in HT1080 parentals. Shown are β-actin (top row), γ-actin (second row), merged (third row) and ratio image (bottom row). **d,** Quantification of the ratio images in **b-c**. Ratios were normalized against the stress fibers. Per cell, 10 data points were collected and in total 15 cells were analyzed over 2 independent experiments. Middle line represents the mean value, and error bars represent standard error of mean (SEM). Statistical analysis was performed using an unpaired t-test P=<0.0001. **e,** Representative images in β- and γ-actin IntAct cells of stress fibers (left column) and cell cortex (right column). Shown are ALFA-tag (top row), F-actin (second row), merged (third row) and ratio images (bottom row). **f,** Quantification of the ratio image in **e**. Per cell, 10 data points were collected and in total 10 cells were analyzed over 2 independent experiments. Middle line represents the mean value, and error bars represent SEM. Statistical analysis was performed using an unpaired t-test P=<0.0001.

western blot), anti-γ-actin (#MCA5776GA, Bio-Rad Laboratories, 1:100 for immunofluorescence, 1:1000 for western blot), anti-Flag (#F1804-1MG, Sigma Aldrich, 1:1000 for western blot), anti-AU1 (#NB600-452, Novus biologicals, 1:100 for immunofluorescence), anti-AU5 (#NB600-461, Novus biologicals, 1:100 for immunofluorescence), anti-profilin (#3246, Cell Signaling, 1:1000 for western blot), anti-cofilin (#5175P, Cell Signaling, 1:1000 for western blot). Secondary antibodies conjugated to Alexa647, Alexa568, or Alexa 488 were used (Life Technologies, 1:400 for immunofluorescence). Actin was stained with Alexa-568-conjugated phalloidin (Life Technologies, 1:200), ALFA-tag was stained with anti-ALFA-atto488 conjugate (NanoTag biotechnologies, 1:100 for immunofluorescence).

Generation of overexpression constructs. All overexpression constructs with the internally tagged actins were generated by Gibson assembly (New England Biolabs). Briefly, two PCRs were performed per construct to generate a DNA fragment upstream of the tag and a fragment downstream of the tag. Primers used for the PCR reactions are given in the Supplementary Materials (**Suppl. Table 1**). Both fragments contained the DNA coding for the tag which functions as an overlapping sequence in the Gibson assembly reaction. The pcDNA3.1 vector backbone was linearized using restriction enzymes HindIII and NheI and 100 ng of vector was used in every Gibson assembly. PCR fragments were added in a 1:6 vector:insert molar ratio and all assembly reactions were incubated for 50 degrees for 50 min. Half the product was transformed into Top10 competent bacteria and clones were screened for the correct vectors.

Generation of knock-in cell lines. gRNAs and HDR templates used for the generation of FLAG-, AU1-, AU5-

bioRxiv preprint doi: https://doi.org/10.1101/2021.10.25.465733; this version posted June 9, 2022. The copyright holder for this preprint (which was not certified by peer review) is the author/funder, who has granted bioRxiv a license to display the preprint in perpetuity. It is made available under aCC-BY-ND 4.0 International license.

t- and ALFA-knock-in cells are given in the Supplementary Materials (**Suppl. Table 2**). Lipofectamine 2000 (ThermoFisher, ref. 11668027) was used to transfect the HT1080 cells. To increase the efficacy of the knockin approach we applied a coselection procedure using ouabain as described previously (44). The gRNA and HDR template for mutating the ATP1A1, which leads to ouabain resistance, are given in the Supplementary Materials (**Suppl. Table 2**). Flow cytometery for the respective tags was performed two weeks after the initial transfection to determine the number of positive cells. Subsequently, treatment with 0.75 µM ouabain was started and after two weeks, single clones were generated from the selected cells. Positive clones were selected based on intracellular FACS staining and were further used for immunofluorescence and western blot.

Immunofluorescence. All steps were performed at room temperature. Cells were seeded on coverslips and fixed using 4% PFA for 10 min. Permeabilization was performed with 0.1% Triton X-100 for 5 min. After washing with 1x PBS, the samples were blocked with 20 mM PBS+glycin. Primary Ab incubation was performed for 1 hr. Subsequently, samples were washed 3x with 1x PBS and incubated with the appropriate secondary Ab for 1 hr in the dark. The samples were then washed 2x with 1x PBS and 1x with MilliQ. After these washing steps the samples were sealed in Mowiol and dried overnight.

Imaging. Imaging was performed on a Zeiss LSM900 laser scanning confocal microscope and a Leica DMI6000 epifluorescence microscope. Images on the LSM900 were acquired using a 63x 1.4 NA oil objective. Alexa488 was excited at 488 nm and emission light was detected between 490-575 nm. Alexa568 was excited at 561 nm and emission was detected between 555-700 nm. Alexa647 was excited at 640 nm and emmission was detected between 622-700 nm. Raw images were processed using the Zeiss Zen 3.1 blue edition software. Images on the Leica DMI6000 were acquired with an HC PL APO 63x 1.40NA oil objective and a metal halide lamp. Alexa488 was excited between 450-490 nm and emmision light was detected between 500-550nm. Alexa568 was excited between 540 nm and emmision light was detected between 567-643 nm.

Live-cell imaging. Parental and/or ALFA β-actin HT1080 cells were seeded in WillCo wells (WillCo Wells B.V.). The next day, cells were transfected with Lifeact-GFP, Nb-ALFA-GFP or Nb-ALFA-mScarlet together with Lifeact using Lipofectamine 2000 (Invitrogen, lot#1854327). Prior to imaging, DMEM was replaced by imaging medium (HBSS, Ca/Mg, 5% FCS, 25 mM HEPES) and incubated for approximately 10 min. Live cell imaging was performed using a Zeiss LSM880 with Airyscan and data was acquired using a 63x 1.4 NA oil objective. During single color live-cell imaging, Lifeact-GFP and Nb-GFP was excited using a mass beam splitter (MBS) 488 and emission light was collected using a 495-550 band pass/570 long pass (LP) filter. Sequentially imaging was done for Lifeact-GFP together with Nb-mScarlet. Lifeact-GFP and Nb-mScarlet were excited using an MBS 488/561 and emission light was collected using a BP 420–480/BP 495–550 for Lifeact-GFP and emission light was collected using a BP 570-620 + LP 645 for Nb-mScarlet. Time series were collected with a frame interval of 5 s for actin treadmilling and 15 s for colocalization of Lifeact with Nb-mScarlet. Raw images were processed using the Zeiss Zen 2.1 Sp1 software. Image series were analyzed using ImageJ and the Pearson correlation coefficient was calculated using the ImageJ tool Coloc2 (PSF: 3, Costes randomizations 10).

Western blot. For western blot, cells were lysed with 2x Laemmli (5 ml 0.5 M Tris pH 6.8, 8 ml 10% SDS, 4 ml Glycerol, few grains bromophenol blue, 2 ml 2-mercaptoethanol and 1 ml MilliQ). Samples were loaded onto 10% or 15% SDS-PAGE gels for separation. Separation was accomplished by running for approximately 2 hrs at 100 V in 1x Running buffer (100 ml 10x TBS, 10ml 10% SDS and 900 ml MilliQ). Proteins were transferred to PVDF membranes for approximately 1 hr at 100 V in transfer buffer (100 ml 10x TBS, 200 ml MeOH and 700 ml MilliQ). Membranes were blocked in 5% milk (ELK milk powder, Friesland Campina) in TBST (1x TBS, 0.1% Tween20) and incubated with primary antibodies overnight at 4°C while rotating. After three times washing with 1x TBST, membranes were incubated in the dark for 1 hr with secondary antibodies while rotating. Washing with 1x TBST was repeated and subsequently, the protein bands were visualized using a Typhoon FLA 7000 (GE Healthcare). ImageJ was used to analyze the protein bands.

F-/G-actin ratio. Heterozygous FLAG-β-actin knockin clones were seeded and the next day washed in ice-cold PBS and lysed on ice for 10 minutes with F-actin stabilization buffer (0.1 M PIPES pH 6.9, 30% glycerol, 5% DMSO, 1 mM MgSO4, 1 mM EGTA, 1% Triton X-100, 1 mM ATP, protease inhibitor cocktail (Sigma, 11697498001)). The cells were harvested and spun down for 10 minutes at 1,000 g and 4°C. The supernatant was collected and spun down at 16,000 g for 75 minutes at 4°C to separate the G- and F-actin fractions. The supernatant, containing G-actin, was collected and the pellet, containing F-actin, was solubilized in depolymerization buffer (0.1 M PIPES pH 6.9, 1 mM MgSO4, 10 mM CaCl2, 5 µM cytochalasin D, 1% SDS). For the negative control, cells were treated with 1 µM Latrunculin A 30 minutes before lysis to disrupt the F-actin fraction. The F-/G-ratio was determined by western blot analysis.

ALFA tag co-immunoprecipitation. Cells were seeded and the following day, the cells were washed five times with ice-cold PBS. Cells were lysed with ice-cold lysis buffer (10 mM Tris, 150 mM NaCl, 2 mM MgCl2, 2 mM CaCl2, 1% Brij-97), supplemented with 1x protease inhibitor cocktail (Roche, 11697498001) and 0.1 mM PMSF (Sigma-Aldrich, P7626-5G). Cell lysates were centrifugation at 16,000 g for 60 minutes at 4°C. For ALFA tag pulldowns, ALFA-Selector ST beads (NanoTag biotechnologies, N1510) were washed twice with lysis buffer. For input 4% or 5% of the clarified lysate was collected as positive control and diluted in 2x Laemmli buffer. The rest of the sample was combined with the beads and incubated for 1 hour at 4°C with rotation.

bioRxiv preprint doi: https://doi.org/10.1101/2021.10.25.465733; this version posted June 9, 2022. The copyright holder for this preprint (which was not certified by peer review) is the author/funder, who has granted bioRxiv a license to display the preprint in perpetuity. It is made available under aCC-BY-ND 4.0 International license.

After enrichment, the beads were pelleted by centrifugation for 1 minute at 1,000 g, and the supernatant was collected as negative control. The beads were washed five times with lysis buffer and incubated for 20 minutes with 2x Laemmli buffer supplemented 0.2 µM elution peptide (NanoTag biotechnologies, N1520-L) at RT with subtle shaking. The samples were centrifuged for 1 minute at 3,000 g and the supernatant collected as elute sample.

FLAG co-immunoprecipitation. The day before starting the co-immunoprecipitation protocol, BSA- and IgG-coated dynabeads for pre-clearing were prepared by mixing dynabeads slurry (40 µl per sample) with 500 µl PBS/3% BSA or 500 µl PBS with 2.5 µg mouse IgG1 (BioLegend, 400102) respectively. Similarly, BSA-coated dynabeads for the IP itself were prepared by mixing 60 µl dynabeads slurry per sample with 500 µl PBS/3% BSA. FLAG knock-in clones were seeded and when the cells reached full confluency, they were washed once with cold PBS and lysed for 15 minutes at 4°C with 1 ml lysis buffer (1% Brij-97, 10 mM Tris-HCl pH 7.5, 150 mM NaCl, 2 mM MgCl2, 2 mM CaCl2, protease inhibitor cocktail (Sigma, 11697498001)). Cell lysates were collected by scraping and spun down at 16,000 g and 4°C for 75 minutes to remove F-actin. In the meantime, the pre-clear beads were washed once with lysis buffer (with or without 1 mM ATP) and resuspended in a total of 40 µl per sample. The supernatant was pre-cleared for 1 hour at 4°C while shaking, with both the BSA- and IgG-coated beads. After pre-clearing, the beads were removed and 40 µl of the supernatant was collected as input. The rest of the sample was split into two parts, which was supplemented with lysis buffer to a volume of 2 ml. 6 µg of either mouse anti-FLAG (Sigma, F1804) or mouse IgG1 (BioLegend, 400102) was added and samples were incubated for 1 hour at 4°C under rotation. Meanwhile, the IP beads were washed with lysis buffer (with or without 1 mM ATP) and resuspended in a total of 60 µl per sample. The beads were added and the samples were incubated for an additional 2 hours. After washing five times with washing buffer (1% Brij-97, 10 mM Tris-HCl pH 7.5, 150 mM NaCl, 2 mM MgCl2, 2 mM CaCl2, 1 mM PMSF), the beads were eluted in 100 mM glycine pH 3.0 for 5 minutes while rotating. The samples were neutralized by adding 1/10th volume of 1M Tris-HCl pH 8.5 and loaded on 15% SDS-PAGE gels for western blot analysis.

Scratch assay. HT1080 Parental and ALFA-β-actin cells were seeded to 100% confluency and a scratch was made with a 200 µl tip from the top to the bottom of the well. After scratching, the cells were washed 1x with PBS and fresh media was added to the cells. The same position was imaged with a Leica DMI6000 epifluorescence microscope after 0 hrs, 4 hrs and 8 hrs and the images were analyzed using ImageJ.

MTT proliferation assay. HT1080 Parental and ALFA-β-actin cells (10.000 or 20.000) were seeded in a 96-well plate. After 16 hrs of incubation, media was replaced by media containing the tetrazolium dye MTT (0.45 mg/ml). After 2 hrs of MTT incubation at 37C in the CO2 incubator, 150 µl DMSO was added to the cells and incubated for 10 min on an orbital shaker until the crystals were dissolved. The absorbance at 560 nm was determined on a microplate reader (iMark microplate absorbance reader, Bio-Rad).

Image analysis. All image analysis was performed using ImageJ (45). Pearson correlation coefficient was calculated using the ImageJ tool Coloc2 (PSF: 3, Costes randomizations 10). For the ratio analysis, the images were first background subtracted. Next, the β-actin intensity was divided by the γ-actin intensity and the brightness/contrast was set between 0 and 2. For each cell, 10 regions (0.5 µm x 0.5 µm) were drawn for stress fibers or the cell cortex and the mean gray value of these regions was measured. In parental HT1080, the ratios were normalized for the stress fibers. For the IntAct cells, first the individual ratios of β-actin or γ-actin over total actin were calculated. The resulting ratios were again divided to determine the relative enrichment of β-actin or γ-actin in stress fibers and the cell cortex. For representation of the results, these final ratios were normalized to the stress fibers.

Data visualization. All graphs were designed in GraphPad Prism 9.0 (GraphPad Software, Inc.) except for Figure 4c and 4f which were generated with SuperPlotsofData (46).

Statistics. The type of statistical test, n values, and P values are all listed in the figure legends or in the figures. All statistical analyses were performed using Graph Pad Prism or Microsoft Excel, and significance was determined using a 95% confidence interval.

Data availability. All primary data supporting the conclusions made are available from the authors on request.

ACKNOWLEDGEMENTS

We are indebted to NanoTag Biotechnologies GmbH, Göttingen, Germany for providing us with the ALFA nanobody expression construct. The authors further thank the Radboud Technology Center Microscopy of the Radboudumc for the use of their microscopy facilities. This work was financially supported by intramural funding of the Radboudumc and by an NWO KLEIN grant (OCENW.KLEIN.494) awarded to K.D..

AUTHOR CONTRIBUTIONS

All authors performed experiments. E.S. generated the overexpression constructs. S.W., W.B. and W.S. generated the HT1080 knock-in cells. W.B and M.C.Z. performed the co-immunoprecipitation experiments. B.J. performed microscopy experiments. B.J. performed microscopy experiments. M.C.Z. performed the overexpression experiments, live-cell imaging, proliferation and migration experiments. K.D. and M.C.Z. carried out data analysis, prepared all the figures and wrote the manuscript. K.D. conceived and supervised the study.

Bibliography

1. L. R. Andrade. Evidence for changes in beta- and gamma-actin proportions during inner ear hair cell life. *Cytoskeleton (Hoboken)*, 72(6):282–91, 2015.
2. K. M. McHugh, K. Crawford, and J. L. Lessard. A comprehensive analysis of the developmental and tissue-specific expression of the isoactin multigene family in the rat. *Dev Biol*, 148(2):442–58, 1991.
3. D. Tondeleir, D. Vandamme, J. Vandekerckhove, C. Ampe, and A. Lambrechts. Actin isoform expression patterns during mammalian development and in pathology: insights from mouse models. *Cell Motil Cytoskeleton*, 66(10):798–815, 2009.
4. F. Parker, T. G. Baboolal, and M. Peckham. Actin mutations and their role in disease. *Int J Mol Sci*, 21(9), 2020. ISSN 1422-0067 (Electronic) 1422-0067 (Linking). doi: 10.3390/ijms21093371.
5. B. J. Perrin and J. M. Ervasti. The actin gene family: function follows isoform. *Cytoskeleton (Hoboken)*, 67(10):630–4, 2010.
6. S. Baranwal, N. G. Naydenov, G. Harris, V. Dugina, K. G. Morgan, C. Chaponnier, and A. I. Ivanov. Nonredundant roles of cytoplasmic beta- and gamma-actin isoforms in regulation of epithelial apical junctions. *Mol Biol Cell*, 23(18):3542–53, 2012.
7. M. Moradi, R. Sivadasan, L. Saal, P. Luningschror, B. Dombert, R. J. Rathod, D. C. Dieterich, R. Blum, and M. Sendtner. Differential roles of alpha-, beta-, and gamma-actin in axon growth and collateral branch formation in motoneurons. *J Cell Biol*, 216(3):793–814, 2017.

bioRxiv preprint doi: https://doi.org/10.1101/2021.10.25.465733; this version posted June 9, 2022. The copyright holder for this preprint (which was not certified by peer review) is the author/funder, who has granted bioRxiv a license to display the preprint in perpetuity. It is made available under aCC-BY-ND 4.0 International license.

8. A. Chen, P. D. Arora, C. A. McCulloch, and A. Wilde. Cytokinesis requires localized beta-actin filament production by an actin isoform specific nucleator. *Nat Commun*, 8(1):1530, 2017.
9. A. Chen, L. Ulloa Severino, T. C. Panagiotou, T. F. Moraes, D. A. Yuen, B. D. Lavoie, and A. Wilde. Inhibition of polar actin assembly by astral microtubules is required for cytokinesis. *Nat Commun*, 12(1):2409, 2021.
10. V. Dugina, I. Zwaenepoel, G. Gabbiani, S. Clement, and C. Chaponnier. Beta and gamma-cytoplasmic actins display distinct distribution and functional diversity. *J Cell Sci*, 122(Pt 16):2980–8, 2009.
11. E. Pasquier, M. P. Tuset, S. Sinnappan, M. Carnell, A. Macmillan, and M. Kavallaris. gamma-actin plays a key role in endothelial cell motility and neovessel maintenance. *Vasc Cell*, 7: 2, 2015.
12. M. Karakozova, M. Kozak, C. C. Wong, A. O. Bailey, 3rd Yates, J. R., A. Mogilner, H. Zebroski, and A. Kashina. Arginylation of beta-actin regulates actin cytoskeleton and cell motility. *Science*, 313(5784):192–6, 2006.
13. F. Zhang, S. Saha, S. A. Shabalina, and A. Kashina. Differential arginylation of actin isoforms is regulated by coding sequence-dependent degradation. *Science*, 329(5998):1534–7, 2010.
14. P. Vedula, S. Kurosaka, B. MacTaggart, Q. Ni, G. Papoian, Y. Jiang, D. W. Dong, and A. Kashina. Different translation dynamics of beta- and gamma-actin regulates cell migration. *Elife*, 10, 2021.
15. J. A. Cooper. Effects of cytochalasin and phalloidin on actin. *J Cell Biol*, 105(4):1473–8, 1987.
16. J. Riedl, A. H. Crevenna, K. Kessenbrock, J. H. Yu, D. Neukirchen, M. Bista, F. Bradke, D. Jenne, T. A. Holak, Z. Werb, M. Sixt, and R. Wedlich-Soldner. Lifeact: a versatile marker to visualize f-actin. *Nat Methods*, 5(7):605–7, 2008.
17. M. J. Schell, C. Erneux, and R. F. Irvine. Inositol 1,4,5-trisphosphate 3-kinase a associates with f-actin and dendritic spines via its n terminus. *J Biol Chem*, 276(40):37537–46, 2001.
18. B. M. Burkel, G. von Dassow, and W. M. Bement. Versatile fluorescent probes for actin filaments based on the actin-binding domain of utrophin. *Cell Motil Cytoskeleton*, 64(11): 822–32, 2007.
19. M. Melak, M. Plessner, and R. Grosse. Actin visualization at a glance. *J Cell Sci*, 130(3): 525–530, 2017. ISSN 1477-9137 (Electronic) 0021-9533 (Linking). doi: 10.1242/jcs.189068.
20. A. Rocchetti, C. Hawes, and V. Kriechbaumer. Fluorescent labelling of the actin cytoskeleton in plants using a cameloid antibody. *Plant Methods*, 10:12, 2014. ISSN 1746-4811 (Print) 1746-4811 (Linking). doi: 10.1186/1746-4811-10-12.
21. C. R. Schiavon, T. Zhang, B. Zhao, A. S. Moore, P. Wales, L. R. Andrade, M. Wu, T. C. Sung, Y. Dayn, J. W. Feng, O. A. Quintero, G. S. Shadel, R. Grosse, and U. Manor. Actin chromobody imaging reveals sub-organellar actin dynamics. *Nat Methods*, 17(9):917–921, 2020. ISSN 1548-7105 (Electronic) 1548-7091 (Linking). doi: 10.1038/s41592-020-0926-5.
22. V. Brault, U. Sauder, M. C. Reedy, U. Aebi, and C. A. Schoenenberger. Differential epitope tagging of actin in transformed drosophila produces distinct effects on myofibril assembly and function of the indirect flight muscle. *Mol Biol Cell*, 10(1):135–49, 1999.
23. H. Rommelaere, D. Waterschoot, K. Neirynck, J. Vandekerckhove, and C. Ampe. A method for rapidly screening functionality of actin mutants and tagged actins. *Biol Proced Online*, 6: 235–249, 2004.
24. A. Simiczyjew, A. J. Mazur, E. Dratkiewicz, and D. Nowak. Involvement of beta- and gamma-actin isoforms in actin cytoskeleton organization and migration abilities of bleb-forming human colon cancer cells. *PLoS One*, 12(3):e0173709, 2017.
25. A. Simiczyjew, A. J. Mazur, A. Popow-Wozniak, M. Malicka-Blaszkiewicz, and D. Nowak. Effect of overexpression of beta- and gamma-actin isoforms on actin cytoskeleton organization and migration of human colon cancer cells. *Histochem Cell Biol*, 142(3):307–22, 2014.
26. J. Q. Wu and T. D. Pollard. Counting cytokinesis proteins globally and locally in fission yeast. *Science*, 310(5746):310–4, 2005.
27. B. Roberts, A. Haupt, A. Tucker, T. Grancharova, J. Arakaki, M. A. Fuqua, A. Nelson, C. Hookway, S. A. Ludmann, I. A. Mueller, R. Yang, R. Horwitz, S. M. Rafelski, and R. N. Gunawardane. Systematic gene tagging using crispr/cas9 in human stem cells to illuminate cell organization. *Mol Biol Cell*, 28(21):2854–2874, 2017.
28. M. Westphal, A. Jungbluth, M. Heidecker, B. Muhlbauer, C. Heizer, J. M. Schwartz, G. Marriott, and G. Gerisch. Microfilament dynamics during cell movement and chemotaxis monitored using a gfp-actin fusion protein. *Curr Biol*, 7(3):176–83, 1997.
29. A. Drazic, H. Aksnes, M. Marie, M. Boczkowska, S. Varland, E. Timmerman, H. Foyn, N. Glomnes, G. Rebowski, F. Impens, K. Gevaert, R. Dominguez, and T. Arnesen. Naa80 is actin's n-terminal acetyltransferase and regulates cytoskeleton assembly and cell motility. *Proc Natl Acad Sci U S A*, 115(17):4399–4404, 2018.
30. M. Goris, R. S. Magin, H. Foyn, L. M. Myklebust, S. Varland, R. Ree, A. Drazic, P. Bhambra, S. I. Stove, M. Baumann, B. E. Haug, R. Marmorstein, and T. Arnesen. Structural determinants and cellular environment define processed actin as the sole substrate of the n-terminal acetyltransferase naa80. *Proc Natl Acad Sci U S A*, 115(17):4405–4410, 2018.
31. Q. Chen, S. Nag, and T. D. Pollard. Formins filter modified actin subunits during processive elongation. *J Struct Biol*, 177(1):32–9, 2012.
32. L. R. Otterbein, P. Graceffa, and R. Dominguez. The crystal structure of uncomplexed actin in the adp state. *Science*, 293(5530):708–11, 2001.
33. M. Boczkowska, Z. Yurtsever, G. Rebowski, M. J. Eck, and R. Dominguez. Crystal structure of leiomodin 2 in complex with actin: A structural and functional reexamination. *Biophys J*, 113(4):889–899, 2017.
34. A. Einhauer and A. Jungbauer. Affinity of the monoclonal antibody m1 directed against the flag peptide. *J Chromatogr A*, 921(1):25–30, 2001.
35. H. Gotzke, M. Kilisch, M. Martinez-Carranza, S. Sograte-Idrissi, A. Rajavel, T. Schlichthaerle, N. Engels, R. Jungmann, P. Stenmark, F. Opazo, and S. Frey. The alfa-tag is a highly versatile tool for nanobody-based bioscience applications. *Nat Commun*, 10(1): 4403, 2019.
36. P. Vedula and A. Kashina. The makings of the 'actin code': regulation of actin's biological function at the amino acid and nucleotide level. *J Cell Sci*, 131(9), 2018.
37. K. van den Dries, L. Nahidiazar, J. A. Slotman, M. B. M. Meddens, E. Pandzic, B. Joosten, M. Ansems, J. Schouwstra, A. Meijer, R. Steen, M. Wijers, J. Fransen, A. B. Houtsmuller, P. W. Wiseman, K. Jalink, and A. Cambi. Modular actin nano-architecture enables podosome protrusion and mechanosensing. *Nat Commun*, 10(1):5171, 2019.
38. T. Splettstoesser, K. C. Holmes, F. Noe, and J. C. Smith. Structural modeling and molecular dynamics simulation of the actin filament. *Proteins*, 79(7):2033–43, 2011.
39. D. S. Kudryashov and E. Reisler. Atp and adp actin states. *Biopolymers*, 99(4):245–56, 2013.
40. H. Rommelaere, D. Waterschoot, K. Neirynck, J. Vandekerckhove, and C. Ampe. Structural plasticity of functional actin: pictures of actin binding protein and polymer interfaces. *Structure*, 11(10):1279–89, 2003.
41. Z. Wang, M. Grange, S. Pospich, T. Wagner, A. L. Kho, M. Gautel, and S. Raunser. Structures from intact myofibrils reveal mechanism of thin filament regulation through nebulin. *Science*, 375(6582):eabn1934, 2022. ISSN 1095-9203 (Electronic) 0036-8075 (Linking). doi: 10.1126/science.abn1934.
42. S. S. Lam, J. D. Martell, K. J. Kamer, T. J. Deerinck, M. H. Ellisman, V. K. Mootha, and A. Y. Ting. Directed evolution of apex2 for electron microscopy and proximity labeling. *Nat Methods*, 12(1):51–4, 2015. ISSN 1548-7105 (Electronic) 1548-7091 (Linking). doi: 10.1038/nmeth.3179.
43. T. C. Branon, J. A. Bosch, A. D. Sanchez, N. D. Udeshi, T. Svinkina, S. A. Carr, J. L. Feldman, N. Perrimon, and A. Y. Ting. Efficient proximity labeling in living cells and organisms with turboid. *Nat Biotechnol*, 36(9):880–887, 2018. ISSN 1546-1696 (Electronic) 1087-0156 (Linking). doi: 10.1038/nbt.4201.
44. D. Agudelo, A. Duringer, L. Bozoyan, C. C. Huard, S. Carter, J. Loehr, D. Synodinou, M. Drouin, J. Salsman, G. Dellaire, J. Laganiere, and Y. Doyon. Marker-free coselection for crispr-driven genome editing in human cells. *Nat Methods*, 14(6):615–620, 2017.
45. C. A. Schneider, W. S. Rasband, and K. W. Eliceiri. Nih image to imagej: 25 years of image analysis. *Nat Methods*, 9(7):671–5, 2012. ISSN 1548-7105 (Electronic) 1548-7091 (Linking). doi: 10.1038/nmeth.2089.
46. J. Goedhart. Superplotsofdata-a web app for the transparent display and quantitative comparison of continuous data from different conditions. *Mol Biol Cell*, 32(6):470–474, 2021. ISSN 1939-4586 (Electronic) 1059-1524 (Linking). doi: 10.1091/mbc.E20-09-0583.